Process Safety and Environmental Protection 162 (2022) 684–693

Contents lists available at ScienceDirect

Process Safety and Environmental Protection

journal homepage: www.elsevier.com/locate/psep

Heat transfer effects on accelerating rate calorimetry of the thermal runaway of Lithium-ion batteries

Xuanze He[a], Chunpeng Zhao[b], Zhenwen Hu[a], Francesco Restuccia[c], Franz Richter[a], Qingsong Wang[b], Guillermo Rein[a,*]

[a] Department of Mechanical Engineering, Imperial College London, London SW7 2AZ, UK
[b] State Key Laboratory of Fire Science, University of Science and Technology of China, Hefei 230026, China
[c] Department of Engineering, King's College London, London WC2R 2LS, UK

ARTICLE INFO

Article history:
Received 6 March 2022
Received in revised form 8 April 2022
Accepted 8 April 2022
Available online 12 April 2022

Keywords:
Ignition
Fire
Safety
Energy Storage
Calorimetry

ABSTRACT

The thermal runaway of Lithium-ion batteries (LIBs) is a fire hazard. The Accelerating Rate Calorimetry (ARC) device is commonly used to investigate thermal runaway parameters of LIBs by assuming adiabatic conditions. However, this assumption ignores internal heat transfer within the cell and external heat transfer at the cell surface. In this work, we conducted ARC experiments using prismatic $LiCoO_2$ cells of 50 mm in side to study the effect of heat transfer limitations. Results show that the external temperature difference between this cell surface and ARC walls varies between 0 and 1.5 °C before thermal runaway and increases from 10 to 130 °C while thermal runaway occurs. Ignoring external heat transfer causes the heat of reaction of the cell to be underestimated by 12%. To study the internal heat transfer, two models are developed and show that heat transfer causes an internal temperature difference that causes an error of kinetics estimation, and the error grows with cell size. Ignoring heat transfer leads to errors on the thermal runaway parameters quantified by ARC, and these errors could propagate to battery safety design and predictions. This study contributes to designing better ARC experiments and a better understanding of battery safety.

1. Introduction

The Lithium-ion battery (LIB) has become one of the most critical technologies for future electric mobility, energy storage and consumer electronics. The fast-updating LIB technology has increased its power, specific energy, and improved its charging performance to satisfy ongoing market requirements. However, although statistically rare, LIB fires pose hazards that are significantly different to other fire hazards (Diaz et al., 2020), in terms of initiation route (Hu et al., 2021), spread (Fang et al., 2021), duration (Chen et al., 2019), toxicity (Yuan et al., 2020), and suppression (Lisbona and Snee, 2011). Therefore, a better understanding of LIB fires and how to protect people and property is an important technical challenge (Diaz et al., 2020; Panchal et al., 2018; Haji Akhoundzadeh et al., 2021).

Many laboratory methods are employed in thermal investigations for the safety of LIB and its components, including differential scanning calorimetry (DSC) (Wen et al., 2012), C80 micro-calorimeter (Wang et al., 2007), vent sizing package 2 (VSP2) adiabatic calorimeter (Jhu et al., 2012) and accelerating rate calorimetry (ARC) (Feng et al., 2014). The DSC and C80 can study material level, while the VSP2 and ARC can study both material and cell level. Compared to DSC and C80, the advantage of ARC is its larger internal chamber volume, satisfying larger format cells (Feng et al., 2014). Using extended volume accelerating rate calorimetry (EV-ARC), even a module of LIBs can be investigated (The Accelerating Rate Calorimeter (EV-ARC), 2010). The ARC was developed to simulate exothermic chemical reactions from reactive materials by simulating quasi-adiabatic conditions, which are achieved by controlling the calorimeter wall temperatures to match the sample temperature while reactions occur (The Accelerating Rate Calorimeter (EV-ARC), 2010). In ARC experiments, LIB ignition is caused by self-heating, which is caused by spontaneous exothermic reactions. Self-heating ignition is a possible cause of LIB fires, for example in storage or electric vehicles (Diaz et al., 2020).

The ARC was devised by the Dow Chemical Company in the 1970s and was commercialized in 1980 (Townsend and Tou, 1980). This technology was developed to simulate exothermic runaway

* Corresponding author.
E-mail address: g.rein@imperial.ac.uk (G. Rein).

https://doi.org/10.1016/j.psep.2022.04.028
0957-5820/

Nomenclature

T	temperature, °C
t	time, s
k	thermal conductivity, W/m-K
c	specific heat capacity, J/kg-K
L	length, m
$\dot{Q}'''$	heat generation, W/m^3
h	convective heat transfer coefficient, W/m^2-K
Bi	Biot number

Abbreviations

LIB	Lithium-ion battery
ARC	accelerating rate calorimetry
EV-ARC	extended volume accelerating rate calorimetry Accelerating rate calorimetry
HWS	heat-wait-seek

Greeks

α	thermal diffusivity, m^2/s
ρ	density, kg/m^3
β	temperature increase rate, K/s
δ	half cell thickness, m

Subscripts

0	initial
s	cell surface
int	internal
ext	external
p	peak
v	vent
w	wall
c	cell
SH	self-heating
TR	thermal runaway

reactions from hazardous and reactive chemicals at a laboratory scale. When conducting ARC experiments, these chemicals are included in a small metal sample container. The temperatures of ARC walls and the metal container surface are measured. Heat transfer between the metal container and the chemicals causes a temperature difference within the chemicals, a thermal lag and thermal inertia. Therefore, ARC cannot provide its desired adiabatic conditions when using a metal container. The experimental data from ARC must be corrected for the effect of the metal container's heat capacity (Wilcock and Rogers, 1997). If heat transfer is not considered in the data analysis, ignoring the internal temperature difference and thermal lag, a large uncertainty of kinetics estimation would be caused (Tou and Whiting, 1981). This is because the kinetics is calculated using an adiabatic assumption and a lumped temperature model, which are not the real conditions of ARC experiments. The heat loss in ARC experiments was investigated by Sheng et al. Sheng et al. (2020). They found that the convective heat loss through the metal container to surroundings does not have a significant effect on the measurement, but the conductive heat loss through the metal container to its connection causes a 16% lower estimation of the total heat generation by the sample. In summary, ARC has been widely used to study thermal properties and behaviors of chemicals, and the effect of heat transfer due to the metal container has also been evaluated, developed and summarized.

The ARC contains three stages: the first stage to identify the onset of self-heating, the second self-heating stage until thermal runaway, and the third stage of thermal runaway and cooling (The Accelerating Rate Calorimeter (EV-ARC), 2010). In the first stage, the heat-wait-seek (HWS) stage is the most common method to identify the onset of self-heating using a temperature rate of 0.02 ℃/min (Mao et al., 2020) or 0.01 ℃/min (Feng et al., 2014). In HWS stage, ARC heats the sample to the initial setting temperature, and then waits for a stage to detect any temperature increase rate. If the rate is higher than the criteria, ARC turns to self-heating stage. Otherwise, ARC keeps heat-wait-detect by increasing the sample temperature by a given temperature step. There is another preheating method to detect self-heating, namely ramp temperature stage (The Accelerating Rate Calorimeter (EV-ARC), 2010). This stage uses a constant temperature increase rate of 5 ℃/min (Lei et al., 2017), to heat the sample from the initial temperature until self-heating is detected. Some works (Lei et al., 2017; Zhao et al., 2020) prefer this method rather than HWS as it can significantly save experimental time. Once self-heating is detected, ARC aims to keep its wall temperatures matching the sample surface temperature until thermal runaway, so that a adiabatic condition can be simulated.

The conventional use of a standard ARC in the chemical industry makes use of a metal container to hold chemical powders, which only have a small size. Comparatively, a LIB or a cell is much larger and it does not need a container in the ARC experiments. The EV-ARC (extended volume accelerating rate calorimeter) has been widely used in LIB thermal and fire studies, from the material level, a single cell level, and even to small modules (Wang et al., 2019; Feng et al., 2018). The biggest difference between an EV-ARC and a standard ARC is that the container of the standard ARC causes thermal inertia and affects heat transfer, while a cell is directly placed in the chamber of the EV-ARC to avoid thermal inertia and heat transfer due to the metal container. Dahn's group (MacNeil et al., 2002; Richard and Dahn, 1999) first employed the ARC to study the thermal behavior of LIB materials. The heat of reaction of the material's exothermic reactions and their kinetics were quantified based on an adiabatic assumption. The parameters were further used in their model to predict the thermal runaway of a 18650 cell using a 3-step reaction scheme (Hatchard et al., 2001). The onset temperature of self-heating (T_{SH}), venting (T_v) and thermal runaway (T_{TR}), and the peak temperature in the ARC (T_p) were obtained (Chen et al., 2016; Jhu et al., 2011). Based on the adiabatic assumption, the T_p indicates the total heat generation, and was used to estimate the heat of reaction of the cell's thermal runaway reactions (Chen et al., 2016; Jhu et al., 2011). The effective kinetics of the cell was also calculated ignoring internal heat transfer within a cell (Chen et al., 2016; Jhu et al., 2011). Feng et al. Feng et al. (2014) first studied the thermal runaway of large-format LIBs. In addition to obtaining similar results as (Chen et al., 2016; Jhu et al., 2011), they further quantified the temperature of separator melting. In summary, employing the ARC, the critical temperatures, the heat of reaction of the exothermic processes, and effective kinetics can be obtained for LIBs.

These parameters are all based on an adiabatic assumption, which ignores the internal heat transfer (there is no temperature difference within the sample), and the external heat transfer (there is no temperature difference at the boundary). However, the ARC can only provide a quasi-adiabatic condition by minimizing the temperature difference between the ARC walls and the sample, which is

Table 1
Cell properties at 30% SOC used in this study.

Parameters	Value	Sources
Activation Energy, E (kJ/mol)	230.78	(He et al., 2020)
Heat of reaction, ΔH (J/kg)	-3.74E+ 05	(Said et al., 2019)
Pre-exponential factor, A (1/s)	1.11E+ 24	(He et al., 2020)
Reaction order, n_c	1	(Hatchard et al., 2001; He et al., 2021)
Density, ρ (kg/m^3)	2164.7	(He et al., 2020; Said et al., 2019)
Specific heat capacity, c (J/kg-K)	990.0	(Said et al., 2019)
Thermal conductivity, k (W/m-K)	1.08	(Werner et al., 2017)
Bi number, Bi	0.04	(He et al., 2020)

not a real adiabatic condition, because two processes of the ARC could potentially lead to uncertainty when using an adiabatic assumption.

The first is the heating stage in either the HWS stage or ramp temperature stage. When heating a sample, an internal temperature difference would occur depending on the heating rate and the material properties (Hayhurst, 2013; Richter and Rein, 2018). The effective kinetics of a cell or materials were quantified without considering this temperature difference (MacNeil et al., 2002; Chen et al., 2016). However, even a 1 ℃ temperature difference within the sample could lead to a 5% error of the kinetics (Vyazovkin et al., 2011). The uncertainty of the kinetics could propagate and grow when predicting thermal runaway using computational models because the kinetics of activation energy has a sensitivity coefficient 10 times larger than the other modelling parameters (He et al., 2021).

The second process that brings uncertainty is caused by the external heat transfer, due to the temperature difference between ARC and sample surface. In terms of the self-heating stage, although the external temperature difference could be small, the effect of the external temperature difference has never been measured for LIBs. This small difference depends on the reaction rate and may further cause the internal temperature difference within the sample, leading to the uncertainty for kinetics estimation. In addition, the heat of reaction of the sample is estimated based on the T_p and assumes no heat losses. However, when thermal runaway occurs, the ARC cannot maintain its wall temperatures the same as the sample surface temperature (The Accelerating Rate Calorimeter (EV-ARC), 2010). The uncertainty of the heat of reaction is highly dependent on this external temperature difference.

Therefore, it is worth analyzing the heat transfer between the ARC and the sample and quantifying how large the internal and external temperature differences are in ARC experiments. We find that most ARC studies for LIBs used the adiabatic assumption and only cell surface temperature was reported. A few works (Chen et al., 2021; Ren et al., 2018) studied the internal and external heat transfer of LIBs during ARC experiments. Chen et al. (2021) measured and modelled the internal temperature difference between the center and the surface of a small battery module consisting of two pouch cells. The maximum internal temperature difference is as high as 400 ℃ when thermal runaway occurs. Ren et al. (2018) modelled thermal runaway by considering the external heat transfer between ARC walls. The ARC wall temperatures are essential but, unfortunately, current studies have not thoroughly analyzed the limitation of heat transfer on LIB safety parameter measurements during LIB ARC experiments.

This study aims to study the effect of heat transfer limitations on ARC experiments. We first conduct ARC experiments using a prismatic $LiCoO_2$ cell at 30% state of charge (SOC) to obtain both the cell surface temperature and ARC wall temperatures. The heat transfer and the temperature difference between the ARC and the cell during the heating stage are calculated and analyzed. We further derive analytical models to calculate the internal temperature difference within a cell in the heating stage and the self-heating stage. The models quantify the uncertainty of ARC experiments and provide guidelines to manage the thermal effects.

2. Experimental methodology

The Sanyo UF103450P prismatic cell is used because it has been extensively studied in the literature (He et al., 2021, 2020; Said et al., 2019), providing detailed cell properties. The cell has a Lithium Cobalt Oxide ($LiCoO_2$) positive electrode and a graphite negative electrode, with dimensions of 34 mm × 10 mm × 50 mm. Its nominal voltage and nominal capacity are 3.7 V and 1880 mAh, respectively. The cells were cycled to 30% SOC before conducting experiments. Following the specification of Sanyo UF103450P, The cells are charged using a CC-CV process with a constant 1 C-rate current of 1.88 A and a cut-off current of 0.188 A. The discharge has a CC process with a constant 1 C-rate current of 1.88 A. The 30% SOC is selected because this is the SOC allowed when batteries are shipped according to the Packing Instruction 965 (UM 3480) by IATA. The cell physical and chemical parameters at this SOC have also been reported (He et al., 2021), and are shown in Table 1.

The experiments were conducted using the extended volume accelerating rate calorimetry (EV-ARC) (Zhao et al., 2020). The sketch of the ARC is shown in Fig. 1. The EV-ARC is a cylindrical chamber with an inner diameter of 25 cm and a height of 60 cm. The bottom,

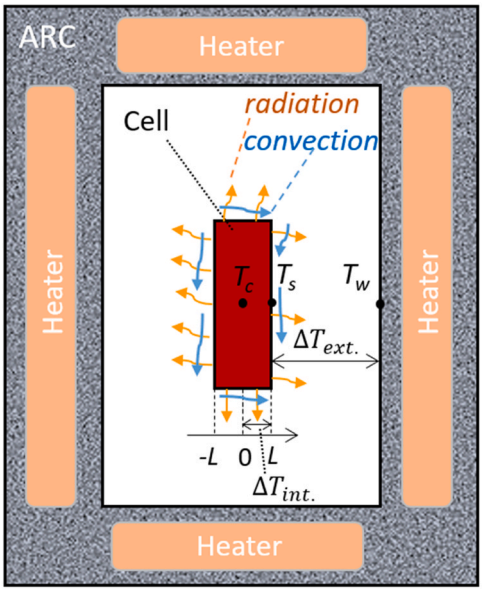

Fig. 1. Sketch of EV-ARC experiments (The Accelerating Rate Calorimeter (EV-ARC), 2010), which has a cylindrical chamber with a heater at the top, bottom, and side walls. We measured the cell surface temperature (T_s) and wall temperature (T_w). During heating stages, ARC controls the wall temperatures, and the cell is heated by radiative and convective heat transfer from the walls. During the self-heating, ARC monitors T_s and heats walls to $T_w = T_s$. There are two temperature differences during the experiment: one external difference ΔT_{ext} and one internal difference ΔT_{int}.

top and sidewall temperatures were monitored by N-type thermocouples. Another N-type thermocouple was attached to the surface of the cell. The cell tab temperature could be different to cell surface temperature when current flows through it. Because an open-circuit cell is used, we only measured the surface temperature.

The experiments followed the HWS stage (Feng et al., 2014). The cell was initially heated to 40 ℃, which is a proper starting temperature because cell internal reactions are negligible at 40 ℃. Then, ARC waited for 60 min to detect the sample temperature increase using a sensitivity of 0.02 ℃/min, which is the most precise sensitivity of the EV-ARC (Zhao et al., 2020). If it failed to detect self-heating, ARC kept conducting HWS stage by increasing the cell temperature by 5 ℃, which is also the experimental error of the onset temperature of self-heating. This temperature step could set smaller but longer experimental time is needed. Using this method, we can only set the temperature step of the heating stage. During multiple HWS stages, when the self-heating rate of 0.02 ℃/min was detected, ARC turned to self-heating stage, in which the ARC traced the temperature of the cell and kept the wall temperatures the same as the cell, until the thermal runaway occurred. The adiabatic condition can be achieved if the ARC wall temperature is exactly equal to the cell surface temperature. However, this is impossible and there is always a small temperature difference between ARC and cell. We aim to study how this small temperature difference during the heating stages in HWS. Overall, In ARC experiments, three critical temperatures of the LIB are measured. T_{SH} is the onset temperature of self-heating using a rate criterion, such as 0.02 ℃/min (Mao et al., 2020). T_{TR} is cell thermal runaway temperature based on a critical temperature increase rate of 10 ℃/min from standard SAE J2464 (SAE J, 2464, 2009). T_p is the maximum temperature. The experiments were repeated twice to capture the experimental uncertainty. The effect of heat transfer on the external temperature difference between cell surface and ARC walls ΔT_{ext} and the internal temperature difference within a cell ΔT_{int} are investigated, as shown in Eqs. (1) and (2).

$$\Delta T_{ext} = T_s - T_w \tag{1}$$

$$\Delta T_{int} = T_s - T_c \tag{2}$$

3. Results

Fig. 2 shows the cell temperature and ARC sidewall temperature during the heat-wait-seek (HWS) stage. During the heating stage, we can see that the ARC wall temperature is significantly larger than the cell temperature. This shows that the cell is heated by convective

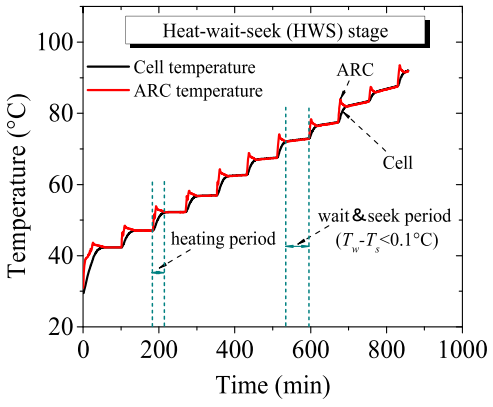

Fig. 2. Measurements of the cell temperature and ARC sidewall temperature during the heat-wait-seek (HWS) stage. The HWS ends when self-heating is detected using the sensitivity of 0.02 ℃/min at the cell temperature of 97 ℃. One heating stage is 20 min, while a wait and seek stage is 60 min. The adiabatic condition is only achieved in the wait and seek stage.

and radiative heat transfer and the effect of heat transfer cannot be ignored. We assume that the Biot number of the cell in the ARC experiments is smaller than 0.1, and therefore the lumped capacitance method (Incropera et al., 2007) can be used to estimate the effective heat transfer coefficient (h). During the heating stage, the internal chemical reactions are negligible because the cell temperature is relatively low. Thus, the temperature increase is due to external heating, and we have Eq. (3) for h based on the lumped capacitance method (Incropera et al., 2007).

$$h = cm\frac{dT_s}{dt}\frac{1}{S}(T_w - T_s) \tag{3}$$

where S is the surface of the cell, c is the heat capacity of the cell, which has been quantified by (Said et al., 2019) shown in Table 1, m is the mass of the cell. Fig. 3(a) gives the plot of dT_s/dt vs $T_w - T_s$ using the temperature data during the heating stage between 190 min and 210 min, showing a linear fit relationship with $R^2 = 0.949$. The slope of this linear fit corresponds to hS/cm, and can be used to calculate the effective heat transfer coefficient. Using this method to calculate the effective heat transfer coefficient in different heating stages, we obtain the $h = 8.5 \pm 0.5 W/m^2K$. Therefore, the cell Biot number in the ARC experiments is shown in Eq. (4).

$$Bi = \frac{hL}{k} = 0.04 \tag{4}$$

where k is the thermal conductivity and L= 0.5 cm is the characteristic length of the cell. The Biot number is smaller than 0.1, which verifies our initial assumption.

During the heating stage, the ARC only controls the temperature step. Fig. 3(b) shows the cell temperature in the HWS stage. The cell temperature in different heating stages overlaps with the parallel straight lines, which justifies that the cell has a constant temperature increase rate in all heating stages. The cell temperature rate in the HWS stage is not set by the ARC before experiments, but it depends on the ARC's actual heating power and the material properties. In our experiments, the cell temperature increase rate β is a constant during heating stages. β = 0.25 ℃/min, as shown in Fig. 3(b). It is important to find that the temperature increase rate of the cell is a constant in the HWS stage, as the rate determines the temperature difference within the cell. This temperature increase is similar to the DSC experiments (Wen et al., 2012), where an internal temperature difference within a sample would occur even for a very small sample (level of mg) (Richter and Rein, 2018). If ARC experiments cause a relatively large internal temperature difference within the cell, the kinetics estimation using the ARC data assuming a lumped capacity would have large uncertainty (Hatchard et al., 2001; Chen et al., 2016; Jhu et al., 2011). This internal heat transfer is analyzed in Section 4.1 of this paper.

During the wait and seek stage, we calculate the temperature difference between the wall and the cell and find T_w-T_s < 0.1 ℃. This shows a negligible external temperature difference, indicating that the adiabatic condition can be reached in the wait and seek stage.

The measurements of cell temperature in the self-heating and thermal runaway stages have been widely reported (Feng et al., 2018), but again, as the adiabatic assumption was used, the temperature difference between the ARC and the cell was ignored in the literature. Fig. 4(a) provides the ARC sidewall temperature and the cell temperature in both the self-heating and thermal runaway stages. The thermal runaway occurred at the time of 990.7 min when cell temperature reached 204.8 ℃. The thermal runaway in this study is defined based on the standard of SAE J2464 using a criterion of 10 ℃/min of cell temperature increase rate. It can be seen from Fig. 4(a) that when this criterion is met, the ARC cannot keep its wall temperatures the same as the cell temperature, because the cell temperature increase rate is too large. The cell temperature rapidly reaches the peak of T_p=330.6 ℃, but the ARC sidewall temperature is

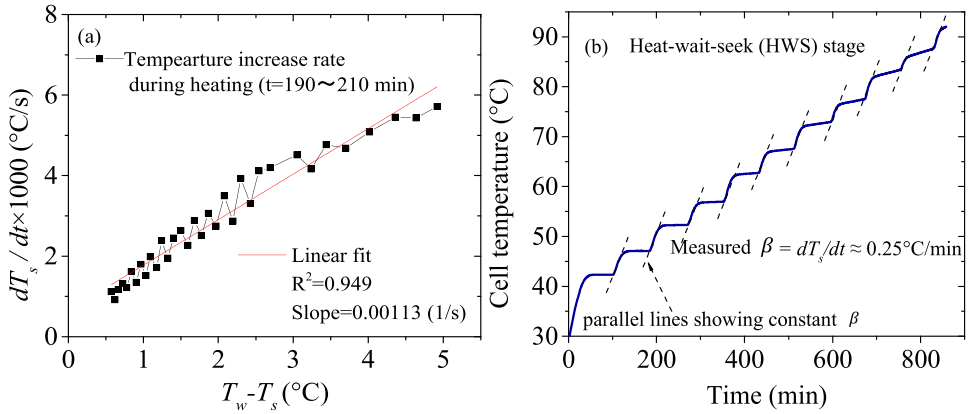

Fig. 3. (a) Extraction of heat transfer coefficient h from the plot of dT_s/dt vs $T_w - T_s$, based on Eq. (3). We used the lumped capacity method based on the ARC wall and cell temperature data during the heating stage. The slope is proportional to h. (b) The cell temperature in the HWS stage. Parallel lines show the constant temperature increase rate during heating.

below 200 ℃. This brings a large uncertainty for the heat of reaction estimation when using an adiabatic assumption. Previous studies (Hatchard et al., 2001; Chen et al., 2016; Jhu et al., 2011; Hayhurst, 2013) assume that heat of reaction is:

$$\Delta H = mc\Delta T_{ad} = mc(T_p - T_{SH}) \tag{5}$$

where ΔT_{ad} is the adiabatic temperature increase, T_{SH} is the onset temperature of self-heating, and T_p is the peak temperature of the cell in the ARC test. Eq. (5) is only achieved when the adiabatic condition is satisfied. But as shown in Fig. 4(a), the temperature difference between the ARC and the cell is quite large. Using adiabatic assumptions to quantify the heat of reaction brings uncertainty due to the neglection of heat transfer (Hatchard et al., 2001; Chen et al., 2016; Jhu et al., 2011).

The temperature difference ($T_s - T_w$) in the self-heating stage is much smaller than that in heating stages. However, it is still not adiabatic. Fig. 4(b) shows the temperature difference between the ARC sidewall and the cell. The temperature increase in this stage is caused by self-heating due to the exothermic reactions rather than the external heating. Therefore, the cell surface temperature is larger than the ARC sidewall temperature. Before venting, the external temperature difference increases with time, and it is smaller than 1.5 ℃. Venting occurred when the cell's internal pressure exceeded the critical pressure of the safety valve at the cell temperature of 167.9 ℃ (Coman et al., 2016). Such a large internal pressure, such as 3448 kPa (Coman et al., 2016), indicates that quick chemical reactions occur, releasing gases and heat. Because of this fast reaction rate, the ARC fails to trace the cell surface temperature. Therefore, the external temperature difference becomes much larger than before venting. The negative value of the external temperature difference is because the venting takes hot gases out of the cell and leads to a decrease of the cell temperature. Data in Fig. 4(b) indicates that when the cell temperature is used to estimate the effective kinetics, the data before venting should be used, rather than the data before the thermal runaway used in previous studies (Chen et al., 2016; Jhu et al., 2011).

The temperatures in ARC experiments are summarized in Table 2. These temperatures are measured based on the cell surface temperature only without considering heat transfer between the ARC and the cell. The temperature difference between T_{SH} in two repeats is 5 ℃, which is the setting temperature step. The classical temperatures between two repeats are very small, showing the good repetition of the ARC experiments. We believe that the ARC is a high-quality technique to quantify critical temperatures of LIBs. However, when analyzing the effective kinetics or the heat of reaction of the cell exothermic process using the ARC data, the effect of external heat transfer between the ARC and the cell, and the internal heat transfer within the cell, must be considered. This is because temperature gradients inside the cell lead to errors in parameter quantification. For example. Vyazovkin et al. (2011) have shown that even a small temperature different of 1 ℃ during an isothermal

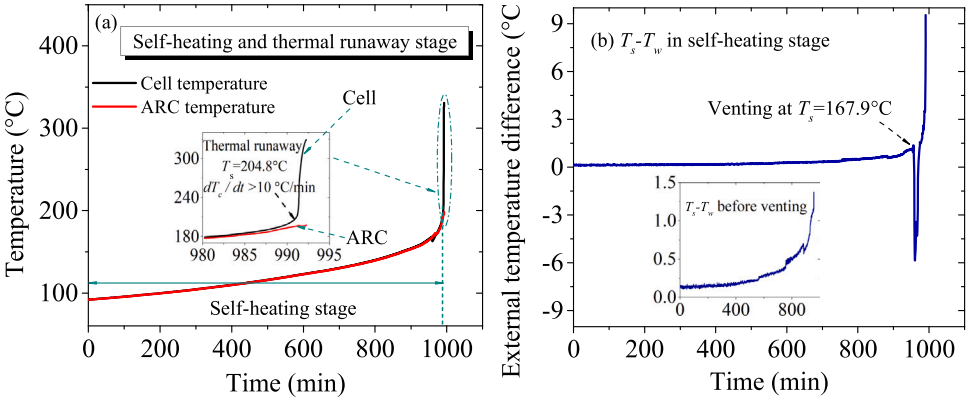

Fig. 4. (a) The cell temperature and ARC sidewall temperature after self-heating is detected using a sensitivity of 0.02 ℃/min. The temperature between the ARC and the cell is significant after the thermal runaway. (b) The temperature difference between the cell and ARC sidewall during the self-heating stage.

Table 2
Results of temperature measurements using ARC. T_{SH} is the onset temperature of self-heating using a sensitivity of 0.02 ℃/min. T_{TR} is the onset temperature of thermal runaway based on the criteria of 10 min/℃ from the standard of SAE J2464 (SAE J, 2464, 2009). T_p is the maximum cell temperature.

Battery	T_{SH} (℃)	T_v (℃)	T_{TR} (℃)	T_p (℃)
Cell 1	92.0	167.9	204.8	330.6
Cell 2	97.0	167.0	202.6	338.7

calorimeter testing can cause a 5% error of the kinetics. This error propagates when using the kinetics in a battery computational simulation.

4. Discussion: the heat transfer limitations

Heat transfer during ARC experiments occurs in two distinct stages. One is the heating stage during either the HWS stage or ramp temperature stage. Another is the self-heating stage. We quantitatively discuss whether heat transfer in both stages leads to large temperature differences within the cell.

4.1. The heating stage

In order to study the internal heat transfer in the heating stage, we develop an analytical model to quantify the maximum temperature difference between the cell surface and the cell center. We use the 1-D heat-diffusion equation for an inert material to analyze the heat transfer. We assume that the exothermic reactions are negligible before self-heating is detected, and the thermal conductivity of the thickness direction is much smaller than other two directions so that we only need to use 1-D model. Thus, the characteristic length of the cell is the half side length, namely $L = 0.5cm$ for the cell we used. Fig. 5 shows the schematic of this 1-D heat transfer problem.

The transient heat conduction governing equation is given by Eq. (6) (Incropera et al., 2007):

$$\frac{\partial T}{\partial t} = \alpha \frac{\partial^2 T}{\partial x^2} \tag{6}$$

where $\alpha = \frac{k}{\rho c}$ is the thermal diffusivity of the cell, k is the thermal conductivity, c is the specific heat and ρ is the density. In the heating stage, the cell temperature increases at a constant rate of β, as shown in Fig. 3(b). Thus, the corresponding boundary condition and the initial condition are given by Eqs. (7) and (8) respectively.

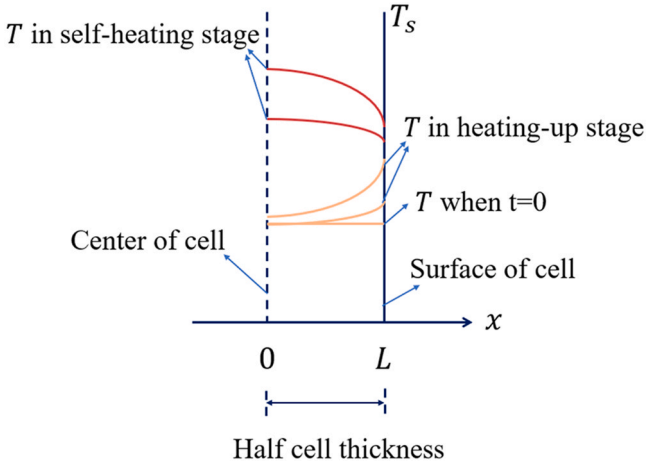

Fig. 5. Schematic of the one-dimensional heat transfer during the heating stage and self-heating stage.

$$T(L, t) = T_s = T_0 + \beta t \tag{7}$$

$$T(x, 0) = T_0 \tag{8}$$

The transient solution of this 1-D heat equation for an inert solid with a constant heating rate boundary condition has been solved by (Carslaw and Jaeger, 1959), the analytical solution is Eq. (9):

$$T(x, t) = T_0 + \beta t + \frac{\beta(x^2 - L^2)}{2\alpha} + \frac{16\beta L^2}{\alpha\pi^3} \sum_{n=0}^{\infty} \frac{(-1)^n}{(2n+1)^3} \times \exp\left[\frac{-\alpha(2n+1)^2\pi^2}{4L^2} t\right] \cos\left[\frac{(2n+1)\pi x}{2L}\right] \tag{9}$$

The temperature difference between the cell surface $T(L, t)$ and the cell center $T(0, t)$ is the parameter we care about. This internal temperature difference is defined as Eq. (10).

$$\Delta T_{int.} = T(L, t) - T(0, t) = \frac{\beta L^2}{2\alpha} + \frac{16\beta L^2}{\alpha\pi^3} \sum_{n=0}^{\infty} \frac{(-1)^n}{(2n+1)^3} \times \exp\left[\frac{-\alpha(2n+1)^2\pi^2}{4L^2} t\right] \cos\left[\frac{(2n+1)\pi}{2}\right] - \frac{16\beta L^2}{\alpha\pi^3} \sum_{n=0}^{\infty} \frac{(-1)^n}{(2n+1)^3} \times \exp\left[\frac{-\alpha(2n+1)^2\pi^2}{4L^2} t\right] \tag{10}$$

The steady state is reached when $t > \frac{4L^2}{\alpha} = 198.4$ s, because the exponential terms tend to 0. This time of 198.4 s is calculated using the parameters shown in Table 1. Based on Fig. 3, each heating stage lasts around 20 min, which is almost an order of magnitude bigger than 198.4 s. This indicates that a steady state is quickly reached during the ARC heating stage. The steady state analytical solution of the internal temperature difference ΔT_{int} becomes Eq. (11). This internal temperature difference is also the maximum temperature difference reached in the steady state during the heating stage.

$$\Delta T_{int} = T(L, t \to \infty) - T(0, t \to \infty) = \frac{\beta L^2}{2\alpha} \tag{11}$$

In terms of a cylindrical cell, such as 18,650 or 21,700, the internal temperature difference is given by Eq. (12), based on the solution for cylindrical conditions from Melling et al. (1969), where R is the radius of the cylindrical cells.

$$\Delta T_{int} = \frac{\beta R^2}{4\alpha} \tag{12}$$

From Eq. (11), we can see that the internal temperature difference ΔT_{int} is controlled by the characteristic length, the heating rate and the thermal diffusivity. The heating rate is controlled by the ARC procedure. In the HWS stage, the heating rate in our ARC experiments is 0.25 ℃/min as shown in Fig. 3(b), while in terms of ramp temperature stage, the heating rate of 2.5 ℃/min (Zhao et al., 2020) and 5 ℃/min (Lei et al., 2017) were used. A larger heating rate can also be set in ARC but it could lead to a large internal temperature difference, based on Eq. (12). The characteristic length of prismatic cells can vary from 0.5 cm (the small cell used in this study) to 3.5 cm (the large cell used for electric vehicles). Moreover, the EV + ARC has a larger internal chamber, which is designed for the small LIB module tests with an even larger size (The Accelerating Rate Calorimeter (EV-ARC), 2010). The ΔT_{int} is propositional to the cell characteristic length, and therefore a larger temperature difference occurs when testing a larger cell using ARC.

In the heating stage, we want to avoid a large internal temperature difference. Here, we select an acceptable internal temperature difference value of 1 ℃, which could cause an error of up to 5% in the kinetics estimation (Vyazovkin et al., 2011). Thus, we can

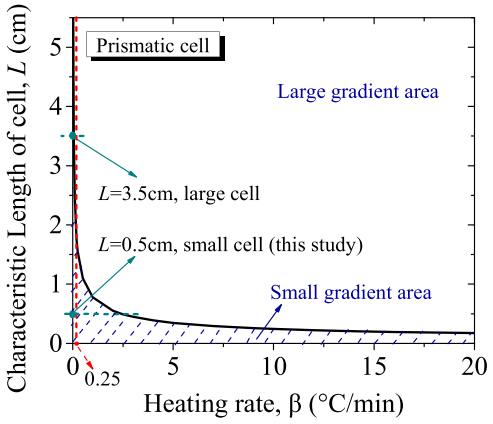

Fig. 6. The characteristic length against the heating rate for a internal temperature difference of 1 ℃ during the heating stage of ARC experiments. The area below the threshold line is the small internal temperature difference area, highlighted using dash lines. This figure provides guidelines for the ARC experiments to avoid generating a large internal temperature difference.

obtain the dependence of the characteristic length and the heating rate using Eq. (11). Fig. 6 shows this dependence. The area below the threshold line corresponds to a small internal temperature difference area, which is highlighted using dash lines using Eq. (7). In terms of the small cell with $L = 0.5cm$, the HWS stage would not bring a large internal temperature difference. However, if the ramp temperature stage is used with a increase rate larger than 2.5 ℃/min, it would cause a large internal temperature difference. Regarding the large cell with $L = 3.5cm$, it seems that an internal temperature difference larger than 1 ℃ is inevitable, the only exception being using the ramp temperature stage setting a temperature increase rate smaller than 0.01 ℃/min. But this would result in a much longer experimental time. Although this internal temperature difference could decrease in the following self-heating stage, it could affect the onset temperature of self-heating T_{SH}.

Fig. 6 can provide guidelines for ARC experiments to avoid the large internal temperature differences during the heating stage. In summary, the HWS stage is suggested for small cell with thickness smaller than 2 cm using ARC experiments. If the ramp temperature stage is selected, the heating rate needs to be calculated using Eq. (11) or Eq. (12) before experiments are carried out. For the large cells, the HWS is not an ideal stage, as the ARC cannot control the heating rate when heating the cells. The ramp temperature stage is therefore suggested, while setting a small enough heating rate to avoid a large internal temperature difference.

4.2. The self-heating stage

The self-heating stage also involves heat transfer. In this stage, the ARC controls the wall temperature matching the cell surface temperature, but there is still a small internal temperature difference (ΔT_{ext}), which dominates the external heat transfer and potentially causes the temperature gradience within the cell.

The cell temperature increase in this stage is caused by self-heating due to the exothermic reactions inside the cell rather than the external heating by the ARC walls. Due to the exothermic reactions, the temperature profile is shown in Fig. 5. The governing equation for this transient self-heating problem is Eq. (13) that is Eq. (1) adding the heat generation term (Incropera et al., 2007), where $\dot{q}$ is the volumetric heat generation.

$$\frac{\partial T}{\partial t} = \alpha \frac{\partial^2 T}{\partial x^2} + \frac{\alpha}{k}\dot{q} \tag{13}$$

The corresponding two boundary conditions and one initial condition of the specific ARC self-heating stage are given by Eqs. (14–16). The boundary conditions at $x = \pm L$ are special because the external temperature difference is small and can be regarded as a constant before venting. Eq. (14) is because of a symmetry temperature profile. Eq. (15) describes a convection boundary condition to the wall.

$$\left.\frac{dT}{dx}\right|_{x=0} = 0 \tag{14}$$

$$\left.\frac{dT}{dx}\right|_{x=\pm L} = \frac{h}{k}(T_s - T_w) = \frac{h}{k}\Delta T_{ext} \tag{15}$$

$$T(x, 0) = T_0 \tag{16}$$

An exact analytical solution to this self-heating problem of Eq. (13) with boundary conditions of Eqs. (14–16) is not available (Bowes, 1984). A numerical approach is needed to model the ARC. In this part, we aim to analyze this problem using an approximate solution, helping understand the internal temperature difference during self-heating.

To solve Eq. (13), we assume that a general solution for the parabolic 1-D temperature distribution. The general solution assumed is in the form of Eq. (17), which has also been used to analyze similar self-heating and heat transfer problems (Lyon et al., 2012). The coefficients of C_1, C_2 and C_3 are to be determined.

$$T(x, t) = C_1 x^2 + C_2 t + C_3 \tag{17}$$

We assume that the heat generation rate $\dot{q}$ is only a function of temperature.

We assume that the temperature increase rate is constant. Therefore, the C_2 is a constant rather than a time-dependent parameter. This is a very good approximation when cell temperature is smaller than 130 ℃, as shown in Fig. 7. Although the heat generation rate $\dot{q}$ of the cell follows the Arrhenius law, it is small if the cell temperature is much smaller than its thermal runaway temperature. As shown in Table 1, the cell in this work has an activation energy of 230.78 kJ/mol, which means that the reaction rate becomes significant only if cell temperature is near the thermal runaway temperature of 204.8 ℃. When cell temperature is smaller than 130 ℃, even though the reaction rate follows the Arrhenius law, it is very small, leading to a very slow temperature increase. We assume the cell temperature increase rate is constant when cell temperature is smaller than 130 ℃, which is the onset separator melting temperature. Fig. 7 shows that the temperature of the cell follows an approximated linear increase with $R^2 = 0.987$. This assumption allows

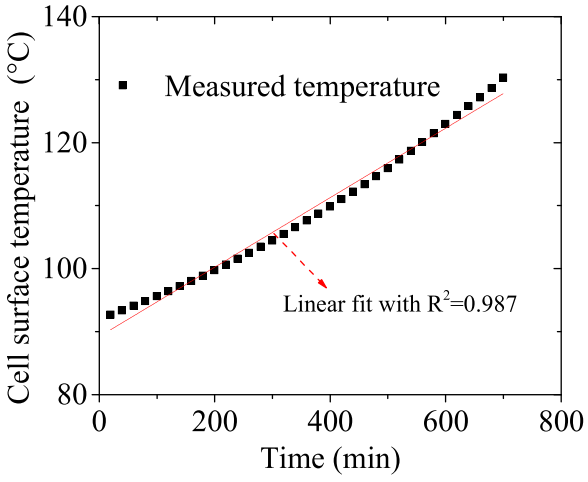

Fig. 7. The cell surface temperature before reaching 130 ℃, which is the onset chemical reaction temperature quantified in the isothermal oven experiments for the same cell (He et al., 2020). The $R^2 = 0.987$ shows that the temperature increase rate can be approximately a constant in this temperature range.

an analytical solution, which helps us better understand the internal heat transfer. The assumption brings an error to cell temperature as shown in Eq. (23), but does not affect the internal temperature difference as shown in Eq. (24), which is the most important research question in this work.

We need to calculate the constants of C_1, C_2 and C_3, based on Eqs. (14–17). The temperature rate at any location x is Eq. (18). The temperature rate β_{SH} is constant according to Fig. 7. The value of the β depends on the volumetric heat generation rate β_{SH}~$\dot{q}$.

$$\frac{\partial T}{\partial t} = C_2 = \beta_{SH} \tag{18}$$

The heat transfer at the boundary $x = \pm L$ is Eq. (19). Thus, we can have C_1 in Eq. (20).

$$\left.\frac{dT}{dx}\right|_{x=\pm L} = 2C_1 L = \frac{h}{k}\Delta T_{ext} \tag{19}$$

$$C_1 = \frac{\Delta T_{ext} h}{2kL} \tag{20}$$

Substituting C_1 and C_2 into Eq. (17), the temperature distribution becomes Eq. (21). As the temperature increase rate at the boundary is a constant, we can apply the temporal boundary condition, $T_s = T_0 + \beta_{SH} t$, and the initial condition of Eq. (17) into Eq. (21). Then, we can find C_3, as shown in Eq. (22).

$$T(x, t) = \frac{\Delta T_{ext} h}{2kL} x^2 + \beta_{SH} t + C_3 \tag{21}$$

$$C_3 = T_0 - \frac{\beta_{SH}}{2\alpha} L^2 \tag{22}$$

Substituting C_3 into the Eq. (21), we can finally have the general solution Eq. (23) for this self-heating problem, where the temperature increase rate is due to self-heating, β_{SH}~$\dot{q}$.

$$T(x, t) = \frac{\Delta T_{ext} h}{2kL} x^2 + \beta_{SH} t + T_0 - \frac{\beta_{SH}}{2\alpha} L^2 \tag{23}$$

Similarly to the previous section, we aim to understand the temperature difference between the cell surface and the cell center. The internal temperature difference is given by in Eq. (24), which depends on the Biot number of the cell and ΔT_{ext}. Due to the 3rd assumption, Eq. (24) can only be used to analyze the internal temperature difference before venting. After venting, as the external temperature difference between the ARC and the cell surface becomes much larger, it causes a larger internal temperature difference within the cell, and affects external heat transfer.

$$\Delta T_{int} = \quad T(L, t) - T(0, t) = \frac{\Delta T_{ext} hL}{2k} = \frac{1}{2}\Delta T_{ext} Bi \tag{24}$$

Based on Eq. (24), Fig. 8 shows that the dependence of the external temperature difference between the ARC and the cell surface against the Biot number during the self-heating stage assuming a maximum internal temperature difference of 1 ℃. The Biot number of the cell in this study is 0.04, as shown in Table 1. For large cells, the Biot number would be smaller than 1 even for the worst case. The line indicates that the internal temperature difference within the cell is always small enough if the ARC can control ΔT_{ext} smaller than 2 ℃, which is calculated by assuming $\Delta T_{int} < 1$℃ and $Bi = 1$ in Eq. (24). In Fig. 4(b), the ARC experiments in this study can always keep the ΔT_{ext} smaller than 1.5 ℃ before venting. Specifically, for the small cell used in this work, the maximum ΔT in the self-heating stage before venting is 0.03 ℃, which is a negligible value. The area below the line contains small internal temperature differences, indicating that the weak heat transfer during the self-heating stage is negligibly.

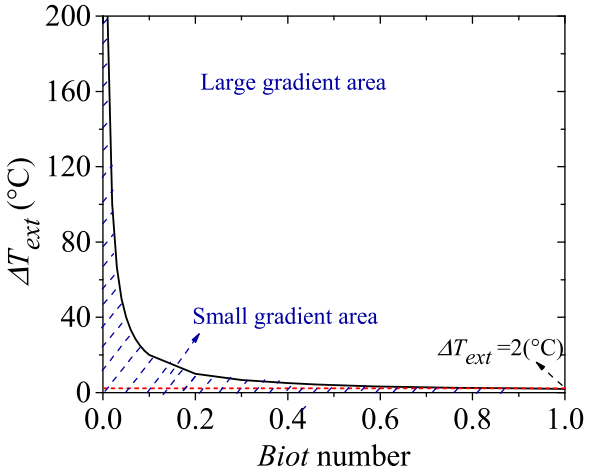

Fig. 8. The calculated ΔT_{ext} against the Biot number in the self-heating stage, assuming a maximum ΔT_{int} of 1 ℃. The area below the threshold line means the small internal temperature differences. The dashed line shows that the internal temperature difference is always small, when the ARC can control the temperature difference smaller than 2 ℃, which is calculated by assuming $\Delta T_{int} < 1$℃ and $Bi = 1$ in Eq. (24).

However, when the ΔT_{ext} is larger than 10 ℃ after venting, even if the internal temperature difference is still small, the large ΔT_{ext} affects external heat transfer, leading to uncertainty when using the adiabatic assumption. Analysis for the process after venting is beyond our scope.

4.3. Heat transfer limitations and parameter quantification

As mentioned in the introduction, all parameters, critical temperatures, heat of reaction of exothermic process, and the effective kinetics quantified by ARC experiments are based on the adiabatic assumption, which is actually not the operating condition of the ARC. In this part, we discuss how the external and internal heat transfer affect these parameters and what could be the error induced.

The external and internal heat transfer causes errors in the cell thermal runaway temperature T_{TR} and the kinetics, however, as mentioned in Section 4.2, these errors are caused by transient heat transfer, where there is no analytic solution to quantify the error. The uncertainty for the kinetics and T_{TR} needs a computational model. This uncertainty is of importance to battery safety and parameter quantification, as a previous study found that a small internal temperature difference of 1 ℃ within the cell could lead to a 5% error in the values of the kinetics (Vyazovkin et al., 2011).

The error of the onset temperature of self-heating (T_{SH}) is dominated by the internal temperature difference within the cell. Therefore, the error of T_{SH} is 0.1℃, which is acceptable for our cell, as shown in Eq. (25).

$$\Delta T_{int} = \frac{\beta L^2}{2\alpha} = 0.1℃ \tag{25}$$

However, we still need to pay attention to the larger cells or when using a large heating rate. Fig. 6 has shown that a large cell or a large heating rate could bring a much larger internal temperature difference and Fig. 6 also provides the guidelines to avoid this.

The heat of reaction of the exothermic process is mainly affected by the external heat transfer. As shown in Fig. 4, after venting, there is a large external temperature difference, especially when thermal runaway occurs. The heat of reaction (8694.5 J) is estimated by $cm(T_p - T_{SH})$ assuming an adiabatic condition. However, the heat losses should be considered, and therefore the heat of reaction is

1080.3 J, as calculated in Eq. (26). Thus, we can see, the heat of reaction is underestimated by 12.4%, which is a large error.

$$cm(T_p - T_{SH}) + h(T_c - T_w)St = 1080.3 \quad \text{J} \tag{26}$$

The T_p is also underestimated due to heat losses. Based on the heat of reaction of 1080.3 J, the actual adiabatic $T_{p,ad}$=360.3 ℃, which is 30 ℃ larger than our experimental data.

Venting occurs during self-heating when a cell's internal pressure reaches a critical value (Coman et al., 2016). The measurement error of external temperature difference is 1.5 ℃ as shown in Fig. 4. The internal temperature difference is smaller than 0.1 ℃, based on Eq. (24). Thus, the measurement uncertainty on venting temperature is not significant. Time to thermal runaway is also affected by heat transfer and it would be the smallest for adiabatic conditions.

There are different types of ARC systems, such as VSP2 (Jhu et al., 2011) and ARC (Zhao et al., 2020). These ARC systems suffer the same measurement errors, because they all assume an adiabatic condition and ignore the effects of heat transfer. The measurement errors vary because different ARC systems have different boundary conditions and temperature control accuracy. It is important for ARC users to recognize the effect of heat transfer. We therefore recommend that ARC data should always be calibrated to take into account heat transfer effects, to minimize measurement errors.

5. Conclusions

This study investigates the effect of internal and external heat transfer on LIB ARC experiments using prismatic cells. Results show that during the external heating stage, the ARC heats the cell with a heat transfer coefficient of 8.5W/m^{2}K, resulting in the increase of temperature at a constant rate of 0.25 ℃/min. When there is no external heating, the ARC minimizes the temperature difference between its walls and the cell (ΔT_{ext}) to minimize the external heat transfer, but it is not an adiabatic condition. We find that the ΔT_{ext} varies between 0 ℃ and 1.5 ℃ before thermal runaway, and it increases to 10 ℃ when thermal runaway occurs and further reaches the maximum temperature of 130 ℃. We develop analytical models to study the internal heat transfer caused. The difference in the heating stage is controlled by the characteristic length, heating rate, and thermal diffusivity. This difference is larger than 1 ℃ when studying large cells with a thickness larger than 7 cm. The difference caused in the self-heating stage is dominated by the ΔT_{ext} and the Biot number. This difference is negligible before venting, because the ΔT_{ext} is small enough in the self-heating stage. But it increases significantly to 2.6 ℃ when thermal runaway occurs for the small cell with a thickness of 10 mm. These two models can provide guidelines for carrying out ARC experiments to avoid large internal temperature differences.

In this work, we find heat transfer is important in ARC experiments. Both the external heat transfer and internal heat transfer are not negligible, and it is necessary to use the adiabatic assumption carefully when quantifying thermal runaway parameters. The results show that heat transfer limitation can lead to errors in the parameters quantified by ARC, especially for large cells. Ignoring heat transfer causes the heat of reaction to be underestimated by 12.4% and the maximum temperature of cells to be underestimated by 9%. This study provides useful guidance on the calorimetry of battery safety and help design better ARC experiments to reduce uncertainty, contributing to a better understanding of LIB safety.

Declaration of Competing Interest

The authors declare that they have no known competing financial interests or personal relationships that could have appeared to influence the work reported in this paper.

Acknowledgments

The authors thank the support from the China Scholarship Council (CSC) and the Great Britain-China Educational Trust (GBCET) to XH and ZH.

References

Bowes, P.C., 1984. Self-Heating: Evaluating and Controlling the Hazards. HMSO, London.
Carslaw, H.S., Jaeger, C.J., 1959. Conduction of Heat in Solids, second ed. Oxford University Press, Oxford, UK, pp. 104–105.
Chen, M., Ouyang, D., Weng, J., Liu, J., Wang, J., 2019. Environmental pressure effects on thermal runaway and fire behaviors of lithium-ion battery with different cathodes and state of charge. Process Saf. Environ. 130, 250–256. https://doi.org/10.1016/j.psep.2019.08.023
Chen, J., Ren, D., Hsu, H., Wang, L., He, X., Zhang, C., Feng, X., Ouyang, M., 2021. Investigating the thermal runaway features of lithium-ion batteries using a thermal resistance network model. Appl. Energy 295, 117038. https://doi.org/10.1016/j.apenergy.2021.117038
Chen, W.C., Wang, Y.W., Shu, C.M., 2016. Adiabatic calorimetry test of the reaction kinetics and self-heating model for 18650 Li-ion cells in various states of charge. J. Power Sources 318, 200–209. https://doi.org/10.1016/j.jpowsour.2016.04.001
Coman, P.T., Rayman, S., White, R.E., 2016. A lumped model of venting during thermal runaway in a cylindrical lithium cobalt oxide lithium-ion cell. J. Power Sources 307, 56–62. https://doi.org/10.1016/j.jpowsour.2015.12.088
Coman, P.T., Rayman, S., White, R.E., 2016. A lumped model of venting during thermal runaway in a cylindrical lithium cobalt oxide lithium-ion cell. J. Power Sources 307, 56–62. https://doi.org/10.1016/j.jpowsour.2015.12.088
Diaz, L.B., He, X., Hu, Z., Restuccia, F., Marinescu, M., Barreras, J.V., Patel, Y., Offer, G., Rein, G., 2020. Meta-review of fire safety of lithium-ion batteries: industry challenges and research contributions. J. Electrochem. Soc. 167 (9), 090559. https://doi.org/10.1149/1945-7111/aba8b9
Fang, J., Cai, J., He, X., 2021. Experimental study on the vertical thermal runaway propagation in cylindrical Lithium-ion batteries: effects of spacing and state of charge. Appl. Therm. Eng., 117399. https://doi.org/10.1016/j.applthermaleng.2021.117399
Feng, X., Fang, M., He, X., Ouyang, M., Lu, L., Wang, H., Zhang, M., 2014. Thermal runaway features of large format prismatic lithium ion battery using extended volume accelerating rate calorimetry. J. Power Sources 255, 294–301. https://doi.org/10.1016/j.jpowsour.2014.01.005
Feng, X., Ouyang, M., Liu, X., Lu, L., Xia, Y., He, X., 2018. Thermal runaway mechanism of lithium ion battery for electric vehicles: a review. Energy Storage Mater. 10, 246–267. https://doi.org/10.1016/j.ensm.2017.05.013
Haji Akhoundzadeh, M., Panchal, S., Samadani, E., Raahemifar, K., Fowler, M., Fraser, R., 2021. Investigation and simulation of electric train utilizing hydrogen fuel cell and lithium-ion battery. Sustain. Energy Technol. Assess. 46, 101234. https://doi.org/10.1016/j.seta.2021.101234
Hatchard, T.D., MacNeil, D.D., Basu, A., Dahn, J.R., 2001. Thermal model of cylindrical and prismatic lithium-ion cells. J. Electrochem. Soc. 148 (7), A755–A761. https://doi.org/10.1149/1.1377592
Hayhurst, A.N., 2013. The kinetics of the pyrolysis or devolatilisation of sewage sludge and other solid fuels. Combust. Flame 160 (1), 138–144. https://doi.org/10.1016/j.combustflame.2012.09.003
He, X., Hu, Z., Restuccia, F., Yuan, H., Rein, G., 2021. Self-heating ignition of large ensembles of Lithium-ion batteries during storage with different states of charge and cathodes. Appl. Therm. Eng. 197, 117349. https://doi.org/10.1016/j.applthermaleng.2021.117349
He, X., Restuccia, F., Zhang, Y., Hu, Z., Huang, X., Fang, J., Rein, G., 2020. Experimental study of self-heating ignition of lithium-ion batteries during storage and transport: effect of the number of cells. Fire Technol. 56 (6), 2649–2669. https://doi.org/10.1007/s10694-020-01011-y
Hu, Z., He, X., Restuccia, F., Yuan, H., Rein, G., 2021. Numerical study of scale effects on self-heating ignition of lithium-ion batteries stored in boxes, shelves and racks. Appl. Therm. Eng. 190, 116780. https://doi.org/10.1016/j.applthermaleng.2021.116780
Incropera, F.P., DeWitt, D.P., Bergman, T.L., Lavine, A.S., 2007. Fundamentals of Heat and Mass Transfer. Wiley.
Jhu, C.Y., Wang, Y.W., Shu, C.M., Chang, J.C., Wu, H.C., 2011. Thermal explosion hazards on 18650 lithium ion batteries with a VSP2 adiabatic calorimeter. J. Hazard. Mater. 192 (1), 99–107. https://doi.org/10.1016/j.jhazmat.2011.04.097
Jhu, C.Y., Wang, Y.W., Wen, C.Y., Shu, C.M., 2012. Thermal runaway potential of $LiCoO_2$ and $Li(Ni1/3Co_{1/3}Mn_{1/3})O_2$ batteries determined with adiabatic calorimetry methodology (doi.org/). Appl. Energy 100, 127–131. https://doi.org/10.1016/j.apenergy.2012.05.064
Lei, B., Zhao, W., Ziebert, C., Uhlmann, N., Rohde, M., Seifert, H.J., 2017. Experimental analysis of thermal runaway in 18650 cylindrical Li-ion cells using an accelerating rate calorimeter. Batteries 3 (2), 14. https://doi.org/10.3390/batteries3020014
Lisbona, D., Snee, T., 2011. A review of hazards associated with primary lithium and lithium-ion batteries. Process Saf. Environ. 89 (6), 434–442. https://doi.org/10.1016/j.psep.2011.06.022
Lyon, R.E., Safronava, N., Senese, J., Stoliarov, S.I., 2012. Thermokinetic model of sample response in nonisothermal analysis. Thermochim. Acta 545, 82–89. https://doi.org/10.1016/j.tca.2012.06.034

MacNeil, D.D., Lu, Z., Chen, Z., Dahn, J.R., 2002. A comparison of the electrode/electrolyte reaction at elevated temperatures for various Li-ion battery cathodes. J. Power Sources 108 (1–2), 8–14. https://doi.org/10.1016/S0378-7753(01)01013-8

Mao, B., Huang, P., Chen, H., Wang, Q., Sun, J., 2020. Self-heating reaction and thermal runaway criticality of the lithium-ion battery. Int. J. Heat. Mass Transf. 149, 119178. https://doi.org/10.1016/j.ijheatmasstransfer.2019.119178

Melling, R., Wilburn, F.W., McIntosh, R.M., 1969. Study of thermal effects observed by differential thermal analysis. Theory and its application to influence of sample parameters on a typical DTA curve. Anal. Chem. 41, 1275–1286. https://doi.org/10.1021/ac60279a009

Panchal, S., Mathew, M., Fraser, R., Fowler, M., 2018. Electrochemical thermal modeling and experimental measurements of 18650 cylindrical lithium-ion battery during discharge cycle for an EV. Appl. Therm. Eng. 135, 123–132. https://doi.org/10.1016/j.applthermaleng.2018.02.046

Ren, D., Liu, X., Feng, X., Lu, L., Ouyang, M., Li, J., He, X., 2018. Model-based thermal runaway prediction of lithium-ion batteries from kinetics analysis of cell components. Appl. Energy 228, 633–644. https://doi.org/10.1016/j.apenergy.2018.06.126

Richard, M.N., Dahn, J.R., 1999. Predicting electrical and thermal abuse behaviours of practical lithium-ion cells from accelerating rate calorimeter studies on small samples in electrolyte. J. Power Sources 79 (2), 135–142. https://doi.org/10.1016/S0378-7753(99)00055-5

Richter, F., Rein, G., 2018. The role of heat transfer limitations in polymer pyrolysis at the microscale. Front. Mech. Eng. 4, 18. https://doi.org/10.3389/fmech.2018.00018

SAE J2464. Electric and hybrid electric vehicle rechargeable energy storage system (RESS) safety and abuse testing, 2009.

Said, A.O., Lee, C., Liu, X., Wu, Z., Stoliarov, S.I., 2019. Simultaneous measurement of multiple thermal hazards associated with a failure of prismatic lithium ion battery. Proc. Combust. Inst. 37 (3), 4173–4180. https://doi.org/10.1016/j.proci.2018.05.066

Sheng, M., Valco, D., Tucker, C., 2020. Heat loss in accelerating rate calorimetry analysis and thermal lag for high self-heat rates. Org. Process Res. Dev. 25 (1), 108–119. https://doi.org/10.1021/acs.oprd.0c00459

The Accelerating Rate Calorimeter (EV-ARC) Operations Manual Version 1, Thermal Hazard Technology, April 2010. ⟨https://www.thermalhazardtechnology.com/downloads⟩.

Tou, J.C., Whiting, L.F., 1981. The thermokinetic performance of an accelerating rate calorimeter. Thermochim. Acta 48, 21–42. https://doi.org/10.1016/0040-6031(81)87019-0

Townsend, D.I., Tou, J.C., 1980. Thermal hazard evaluation by an accelerating rate calorimeter. Thermochim. Acta 37 (1), 1–30. https://doi.org/10.1016/0040-6031(80)85001-5

Vyazovkin, S., Burnham, A.K., Criado, J.M., Pérez-Maqueda, L.A., Popescu, C., Sbirrazzuoli, N., 2011. ICTAC kinetics committee recommendations for performing kinetic computations on thermal analysis data. Thermochim. Acta 520 (1–2), 1–19. https://doi.org/10.1016/j.tca.2011.03.034

Wang, Q., Mao, B., Stoliarov, S.I., Sun, J., 2019. A review of lithium ion battery failure mechanisms and fire prevention strategies. Prog. Energy Combust. Sci. 73, 95–131. https://doi.org/10.1016/j.pecs.2019.03.002

Wang, Q., Sun, J., Chen, C., 2007. Thermal stability of delithiated LiMn2O4 with electrolyte for lithium-ion batteries. J. Electrochem. Soc. 154 (4), 263–267. https://doi.org/10.1149/1.2433698

Wen, C.Y., Jhu, C.Y., Wang, Y.W., Chiang, C.C., Shu, C.M., 2012. Thermal runaway features of 18650 lithium-ion batteries for LiFePO4 cathode material by DSC and VSP2. J. Therm. Anal. Calorim. 109 (3), 1297–1302. https://doi.org/10.1007/s10973-012-2573-2

Werner, D., Loges, A., Becker, D.J., Wetzel, T., 2017. Thermal conductivity of Li-ion batteries and their electrode configurations–a novel combination of modelling and experimental approach. J. Power Sources 364, 72–83. https://doi.org/10.1016/j.jpowsour.2017.07.105

Wilcock, E., Rogers, R.L., 1997. A review of the phi factor during runaway conditions. J. Loss Prev. Process Ind. 10, 289–302. https://doi.org/10.1016/S0950-4230(97)00018-1

Yuan, L., Dubaniewicz, T., Zlochower, I., Thomas, R., Rayyan, N., 2020. Experimental study on thermal runaway and vented gases of lithium-ion cells. Process Saf. Environ. 144, 186–192. https://doi.org/10.1016/j.psep.2020.07.028

Zhao, C., Sun, J., Wang, Q., 2020. Thermal runaway hazards investigation on 18650 lithium-ion battery using extended volume accelerating rate calorimeter. J. Energy Storage 28, 101232. https://doi.org/10.1016/j.est.2020.101232